Article

Combining Gasoline Compression Ignition and Powertrain Hybridization for Long-Haul Applications

Rafael Lago Sari *, Yu Zhang, Brock Merritt, Praveen Kumar and Ashish Shah

Aramco Americas: Aramco Research Center—Detroit, 46535 Peary Ct, Novi, MI 48377, USA;
praveen.kumar@aramcoamericas.com (P.K.)
* Correspondence: rafael.lagosari@aramcoamericas.com

Abstract: Gasoline compression ignition (GCI) combustion was demonstrated to be an effective combustion concept to achieve high brake thermal efficiency with low-reactivity fuels while offering improved NOx–soot trade-off. Nevertheless, future greenhouse gas regulations still challenge the heavy-duty transportation sector on both engine and vehicle basis. Hybridization is a possible solution in this scenario, allowing the avoidance of low-efficiency conditions and energy recovery during regenerative braking, improving overall vehicle efficiency. In this sense, this investigation proposes a detailed analysis to understand the optimum hybridization strategy to be used together with GCI to simultaneously harness low pollutant and CO_2 emissions. For that, different hybrid architectures were defined in GT Drive (Mild hybrid 48 V P0 and P2 and full Hybrid P2 500 V) and submitted to 15 different use cases, constituted by five normative and real-driving conditions from the US, China, India, and Europe and three different payloads. Results showed that all hybridization strategies could provide fuel savings benefits to some extent. Nonetheless, usage profile is a dominant factor to be accounted for, benefiting specific hybrid powertrains. For instance, P0 and P2 48 V could provide similar savings as P2 500 V, where regenerative braking is limited. Nonetheless, P2 500 V is a superior powertrain if more demanding cycles are considered, allowing it to drive and recuperate energy without exceeding the Crate limitations of the battery.

Keywords: gasoline compression ignition; hybrid trucks; transport decarbonization; long-haul trucks

1. Introduction

Class 8 long-haul decarbonization requirements are a reality in several countries worldwide. Despite fewer vehicles than passenger cars, heavy-duty vehicles represent 25% to 30% of the total CO_2 produced in the transportation sector in the US and Europe, respectively [1,2]. In this sense, gradual CO_2 reduction requirements are being introduced to reduce the carbon footprint of this sector and, possibly, transition to a carbon-neutral sector. The United States Environmental Protection Agency proposed a set of targets from a vehicle and engine perspective. Phase 2 requirements include a 222 g/ton-mile limit for the vehicle and 432 g/bhp-h at an engine level. The last represents a reduction of almost 10% compared to 2014 levels [3]. Other important markets, such as Europe, also introduced a roadmap for CO_2 reduction, targeting a 15% reduction from 2025 and 30% from 2030 [4]. In these specific cases, further discussions are taking place to make regulation even more stringent, with a 45% reduction from 2030 and a 65% reduction from 2035.

This scenario challenges industry and academia to develop and introduce technologies capable of enabling CO_2 reduction while preserving vehicle durability, timeliness, and cost. Several combustion and air management technologies have demonstrated success in CO_2 and pollutant emission reduction over the years [5–7]. Ultra-efficient combustion concepts were introduced, demonstrating reliable operation with market-grade and synthetic fuels. Dual-mode dual-fuel combustion (DMDF) was conceived from the combination of reactivity-controlled compression ignition (RCCI) and conventional diffusive combustion [8–10]. While RCCI is explored at low and medium loads, leading to ultra-low NOx

and soot emissions, low-temperature diffusive combustion is used for full-load operation. In this sense, challenges such as high pressure-rise rate and maximum in-cylinder pressure can be mitigated, maintaining diesel characteristics such as low-end torque and power output [11]. DMDF has been validated against different driving conditions and powertrain architectures, demonstrating its ability to be used as a standalone application or with hybrid architectures such as series and parallel ones with different fuels [12,13]. Nonetheless, the requirement for an additional fuel supply is frequently seen as a technological barrier to its implementation. Similarly, gasoline compression ignition is an evolution of former low-temperature combustion concepts, combining pre-mixed combustion at low loads with diffusion combustion at high to full loads to meet the torque and power requirements of a modern diesel engine [14,15]. Unlike RCCI and DMDF, GCI relies on a single low-reactivity fuel for full map operation, with minor hardware modification requirements, and could be seen as an off-the-shelve technology. The higher volatility of gasoline and longer ignition delays provide an efficient lever to improve NOx–soot trade-off while achieving diesel-like efficiency. Different literature reports suggested enhanced GCI operation across various operating conditions, with fuel consumption savings close to 6% [16,17]. In addition, low NOx GCI combustion and air management recipes could also be extended to conventional diesel combustion with similar benefits [18]. The benefits of GCI combustion in the heavy-duty space at steady-state conditions were extensively discussed in the literature. Zhang et al. [19] assessed the implementation of the PPCI-diffusion GCI combustion in a 15 L multicylinder engine at representative conditions of the supplementary engine test (SET) cycle. A thorough evaluation for different compression ratios, injection strategies, and piston designs were performed, aiming at quantifying the impact of such strategies on combustion and emissions of criteria pollutants (NOx, HC, CO, and soot). Overall, GCI was able to deliver improved soot–NOx trade-off while offering diesel-like efficiency levels. Additional investigations also demonstrated the potential of GCI combustion, achieving a 6.3% fuel consumption improvement at the B50 operating condition (B speed as determined by the SET procedure at 50% of engine load at the respective speed) compared to baseline hardware with a dedicated GCI combustion system. Low load operations have also been addressed in the literature, demonstrating that either exhaust rebreathing or spark-assisted operation can be alternatives that provide robust operation under these conditions.

The benefits of GCI could be further extended if combined with powertrain hybridization. Hybrid powertrains are known for providing a direct path to CO_2 reduction through energy recuperation and possible benefits to engine operation [20,21]. While these benefits are evident for passenger cars [22–24], there are indications that hybrid performance and the best hybrid architecture to be used in the medium- and heavy-duty sectors depend heavily on the driving profile and payload requirements [25,26]. Given that the engine is heavily loaded during the driving cycle in most cases, direct engine power output can be more attractive than the energy transfer to batteries and electric motors. Garcia et al. [27] demonstrated the effect of payload and driving conditions on a medium-duty truck under different powertrain architectures. While appreciable benefits were found at 0% and 50% of the payload, the differences for 100% of the payload between hybrid powertrains and conventional diesel trucks were minimal. Zhao et al. [28] also investigated the potential of a parallel hybrid for class 8 trucks under representative conditions. Overall, no significant benefit was achieved for the hybrid powertrain with penalizations in the total purchase cost. Later, Prada et al. [25] assessed the opportunities for heavy-duty fuel consumption improvements through hybridization. They included different driving cycles inside the US and truck classes. In conclusion, the authors found a strong correlation between the driving profile characteristics and the savings in fuel consumption that ranged from 0% to almost 20%, depending on the driving condition. These results indicate that strong hybridization may not be the preferred path depending on the use case.

Despite the literature findings, studies to identify the best powertrain option for different representative markets worldwide in combination with gasoline compression ignition combustion are not available in the literature. In this sense, this investigation

proposes to assess the optimal hybrid powertrain option for class 8 trucks for different countries while operating with GCI as an enabler for low emissions and high fuel efficiency. For that, three powertrain layouts were considered. P0 and P2 48 V powertrains and P2 500 V were assessed under driving cycles from the US, India, China, and Europe using different payloads. The hybrid series was not considered an option in this investigation due to the reported lower efficiency for class 8 trucks [29]. Detailed truck models were built and validated with previous data from the dynamometer using a conventional diesel combustion calibration. The vehicle models (conventional and hybrid GCI concepts) were simulated in different driving conditions, representing normative and real-driving conditions (obtained using GT-real Drive) to understand the effect of the use profile on the powertrain efficiency. Finally, a total vehicle cost analysis was introduced to identify the cost for CO_2 reduction of each powertrain.

2. Materials and Methodology

This section includes a brief description of engine calibration maps and the validation of the map-based approach. Thereafter, vehicle models developed in GT-drive and the different driving conditions are discussed in detail.

2.1. Internal Combustion Engine Description

An MY13 Cummins ISX15 was used as the base engine for the development of this investigation. The main characteristics of this engine are presented in Table 1. This engine was optimized through several iterations on the combustion and air management system to run efficiently and cleanly under low engine-out conditions using gasoline or diesel as fuels as described by [17].

Table 1. Main engine characteristics.

| Engine Characteristics	
Engine Type	**Four-Stroke, Four Valves, Direct Injection**
Number of cylinders [-]	6
Displaced volume [L]	14.9
Stroke [mm]	169
Bore [mm]	137
Rated power and torque	336 kW @ 1800 rpm 2375 Nm @ 1000 rpm
Air-handling system	Single-stage variable geometry turbocharger, cooled HP EGR with charge air cooling

As discussed in the introduction, gasoline compression ignition combustion has demonstrated superior capability in achieving ultra-low NOx and soot results while promoting diesel-like efficiency. Specifically, the PPCI-diffusion strategy previously developed by Zhang et al. [23] allows one to harness the benefits of premixed combustion from a low-to-medium load, while covering full-load operation with a diffusive strategy. Using the strategy described in previous works, a complete map calibration was proposed, targeting the same power output as the original diesel engine. Each point was optimized following one-factor-at-a-time (OFTA) optimization aiming at brake-specific nitrogen oxide (BSNOx) values lower than 2 g/kWh and smoke below 1 FSN. The maps from Figure 1a–c illustrate the final calibration results for brake thermal efficiency, BSNOx, and FSN. It is relevant to remark that the proposed calibration delivered peak efficiency values of 44.7%, equivalent to those from the original diesel calibration (44.8%). Moreover, the overall GCI calibration can deliver BSNOx values close to 1.5 g/kWh in most operating maps without penalizing soot emissions. This means a reduction of more than 3.3 g/kWh BSNOx compared to

the original conventional diesel combustion calibration and a direct reduction in the urea requirements in the NOx after treatment system.
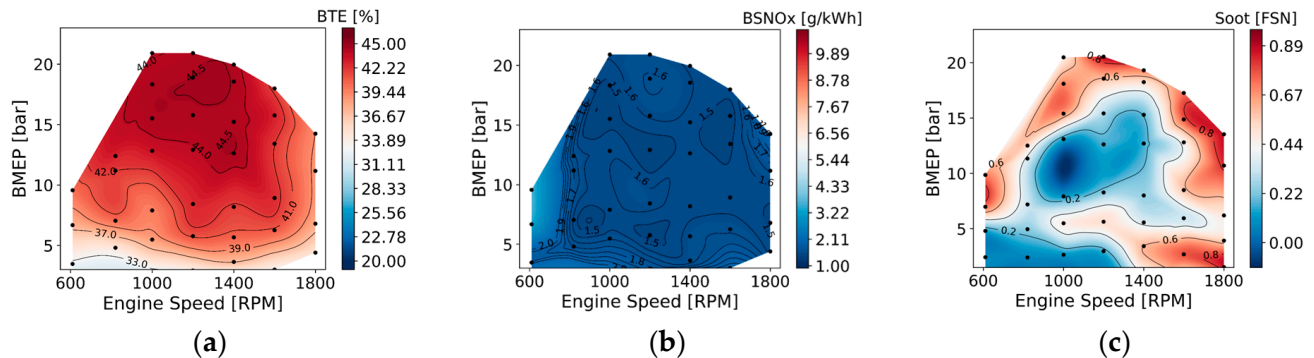
Figure 1. Gasoline compression ignition calibration maps for brake thermal efficiency (**a**), brake-specific nitrogen oxide emissions (**b**), and filter smoke number (**c**).

The correct representation of transient operation in the vehicle model demands an accurate verification of the model and validation against experimental results. To do so, the calibration maps were used as inputs in a simplified engine map-based model in GT-Drive presented in Figure 2.
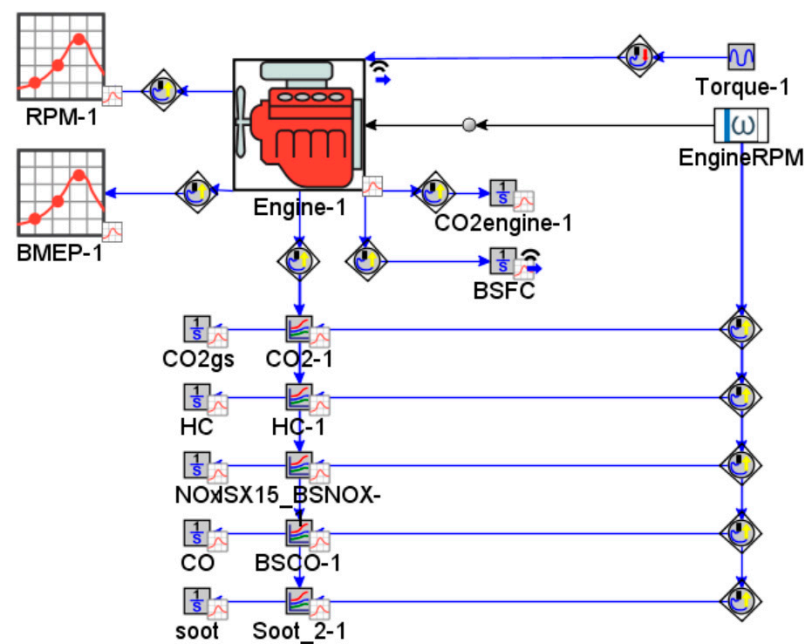
Figure 2. Simplified GT-Drive model to compare the transient response from map interpolation with test-cell transient results.

Next, the torque and engine speed profiles from an FTP dynamometer cycle were imposed in the model to calculate the respective instantaneous values for the cycle from the maps. Finally, these values were compared to the experimental results for fuel consumption, NOx, and CO_2 emissions. As shown in Figure 3, the map-based approach allows for the estimation of the fuel consumption and CO_2 emissions with reasonable accuracy. NOx emissions are also well captured by this approach. Still, higher differences are evidenced in specific points that might be caused by variations in the test's EGR valve area, actuators, or even environmental conditions.
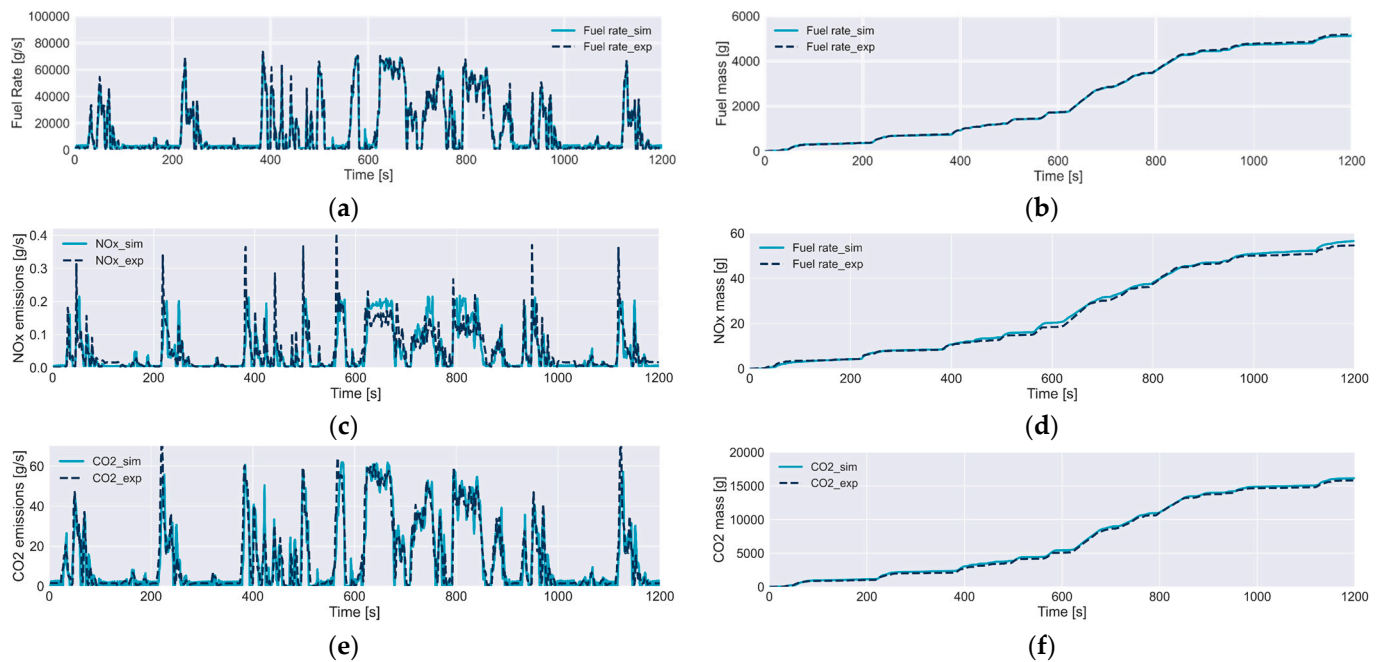
Figure 3. Comparison of experimental and simulated instantaneous values for fuel rate (**a**), NOx emissions (**b**), and CO_2 emissions (**c**), as well as the cumulative values for fuel rate (**d**), NOx emissions (**e**), and CO_2 emissions (**f**).

2.2. Truck Modelling Description and Driving Profiles

GT-Drive was selected as a modelling tool to simulate the different powertrains assessed in this investigation. The powertrains were incorporated in a full vehicle model to enable their evaluation under different driving conditions and payloads. For this evaluation, a VOLVO VNL 760 truck was chosen as the base vehicle considering its representativeness in the long-haul market. The main characteristics of the truck used are presented in Table 2.

Table 2. Main truck characteristics used in the GT-Real Drive models.

Truck Characteristics	
Engine	**ISX15**
Vehicle weight [kg]	8730
Drag coefficient [-]	0.62
Vehicle frontal area [m^2]	6.5
Gross vehicle weight [kg]	36,250
Vehicle wheelbase [m]	5.5
Rolling friction [-]	0.007
Tires specification	295/80R/22.5″
Gearbox models	ATO2612F
Differential drive ratio	2.28

Figure 4a,c represent the different GT-Drive models. The first model represents the conventional powertrain, consisting of an internal combustion engine, transmission, and truck properties. Figure 4b illustrates a 48 V belt-assisted starter (BAS) with a small motor and 48 V battery coupled to the conventional powertrain. This system enables energy recuperation and efficiency improvement through regenerative braking and modification of the operating conditions of the engine towards higher efficiency. Moreover, supervisory controllers and battery management systems are incorporated to define the states and manage their transitions and constrain current demands under the electrochemistry limits of the battery. Figure 4c illustrates the P2 system used for both 48 V and 500 V powertrains. This powertrain introduces fully electric operating modes and torque supply at high loads

as additional features. Two clutches are used to engage or disengage the motor and engine depending on the operation mode.

(**a**)

(**b**)

(**c**)
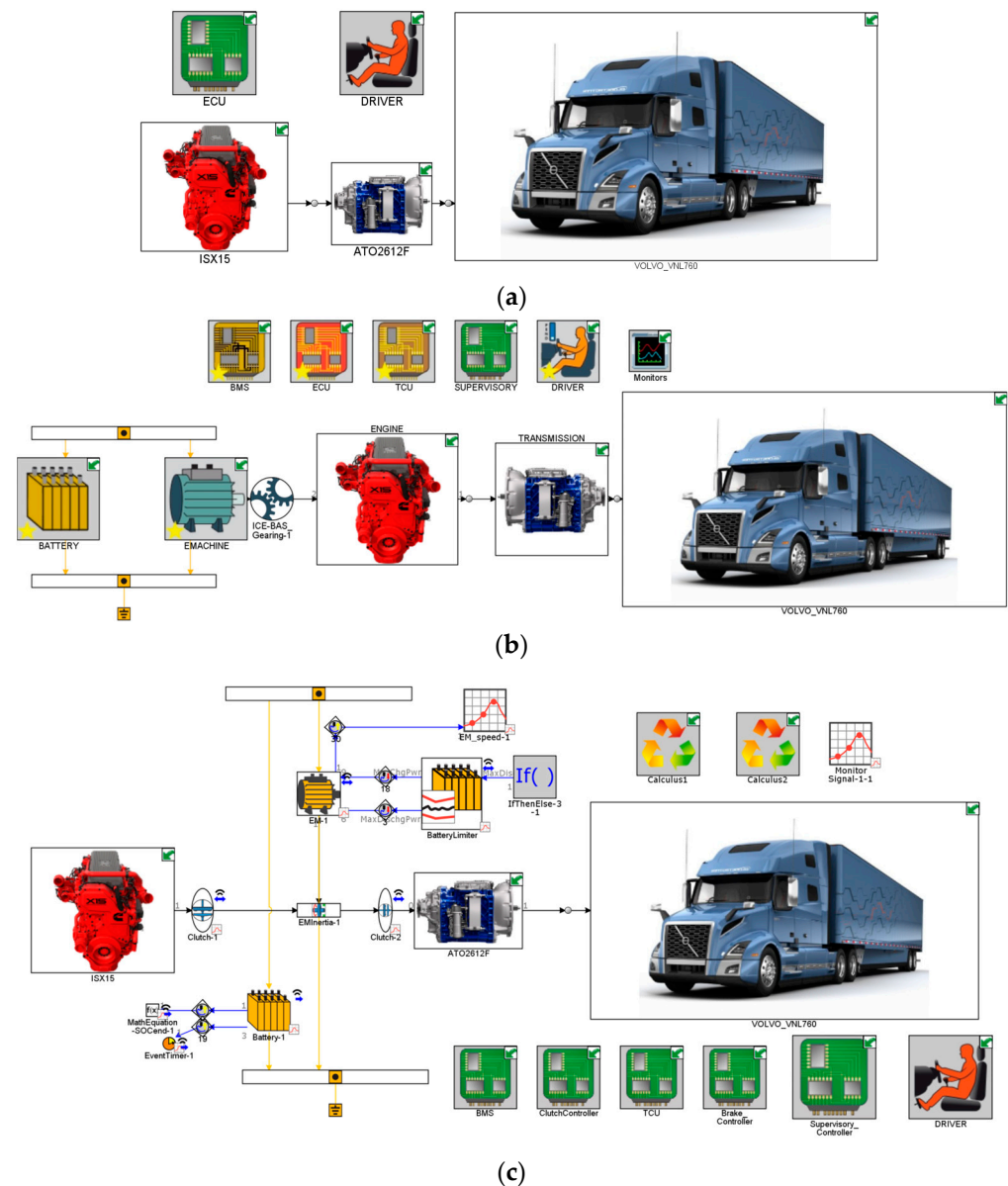
Figure 4. GT-Drive model for the VOLVO FE 350 truck for conventional (**a**), P0 48 V (**b**), and P2 48 V and 500 V (**c**).

Table 3 illustrates the initial sizing of the components used in the powertrain. Additional optimization was performed for the battery size, considering CO_2 and cost minimization as optimization targets. The battery size was later optimized to take into consideration the effect of ohmic losses, regenerative braking capacity, and battery weight. This was attained by sweeping the number of cells in series from 1 to 140. A gear shift strategy optimization was performed for each powertrain option considering the WHVC driving cycle at 50% of the payload and maintained fixed for all the other cycles. The engine speed shifting band was obtained using a direct optimizer based on a genetic algorithm, so the best solution for the gear shifting strategy could be obtained.

Table 3. Initial configuration for the different hybrid powertrains assessed.

Device	P0	P2 48 V	P2 500 V
Traction motor size [kW]	20	50	100
Initial battery [kWh]	6.8	8	20
Final gear ratio [-]	2.25	2.25	2.25
Max Crate 5 s [-]	20	20	20
Max Crate $t > 10$ s [-]	7	7	7

For the longitudinal vehicle model, the required speed and torque to follow the desired vehicle speed were specified. The value of each parameter from the input maps was obtained by interpolation. Equation (1) presents the governing equation that should be solved for each simulation time step where I_{trans1} and I_{trans2} present the inertia in the input and output of the transmission system. Likewise, I_{dsh} and I_{axl} are the driveshafts and axle's moment of inertia. R_d and R_t are terms of the final drive and transmission ratio for each gear. dRT/dt represents the derivative of the transmission ratio. Vehicle speed (ω_{drv}) at an instant of time (t) is directly related to the wheel radius (r_{whl}) and vehicle mass (M_{veh}). Aerodynamic forces (F_d), rolling resistance forces (F_{rol}), and gravity forces (F_{grd}) are considered in the last term of Equation (1). Detailed information can be found in [30]. This approach has demonstrated superior capacity in providing accuracy in predicting the real performance of the engine under driving cycle conditions with reasonable time consumption. Additional details on the modelling approach and accuracy of the model can be found in [8].

$$\tau_{vehicle} = \left[I_{trans1} + \frac{I_{trans2}}{R_t^2} + \frac{I_{dsh}}{R_t^2} + \frac{I_{axl}}{(R_d^2)(R_t^2)} + \frac{(M_{veh})(r_{whl}^2)}{(R_d^2)(R_t^2)} \right] \frac{d\omega_{drv}}{dt}$$
$$- \left[\frac{I_{trans2}}{R_t^3} + \frac{I_{dsh}}{R_t^3} + \frac{I_{axl}}{(R_d^2)(R_t^3)} + \frac{(M_{veh})(r_{whl}^2)}{(R_d^2)(R_t^3)} \right] \omega_{drv} \frac{dR_t}{dt} + \left[\frac{F_{aer} + F_{rol} + F_{grd}}{R_d R_t} \right] r_{whl} \tag{1}$$

Hybrid powertrain systems incorporate two different sources of energy to provide tractive power to the wheel axles: a traction motor and an internal combustion engine. Additionally, the addition of electrical motors enables specific operating modes for the truck, so energy can be utilized in the most efficient path, e.g., electric mode, electrically assisted mode, and regenerative braking. In this sense, the definition of the modes and the control strategy to specify the active mode plays a significant role in the optimization of a hybrid powertrain. Specifically for this study, a rule-based controller (RBC) strategy was selected. The specific modes are described in Table 4 below for each of the powertrains.

Table 4. Operating modes for each hybrid powertrain configuration.

Mode	P0	P2 48 V	P2 500 V
e-Drive	no	yes	yes
e-Assist	yes	yes	yes
Regenerative braking	yes	yes	yes
Engine only	yes	yes	yes

The transition between modes followed pre-established thresholds. For concepts where e-drive was available (traction power was provided only by the traction motor), e-drive was used for conditions where the vehicle speed was low, battery energy was available (SOC > SOC$_{min}$), and axle torque was lower than the torque that could be provided by the traction motor. Once any of these conditions were not satisfied, the supervisory controller changed the operation mode to either e-assist or engine only. Considering the high efficiencies of the combustion concepts used in this investigation, the highest efficiency path prompted the use of ICE over a mixed mode. A mixed use of ICE and traction motor at low torque requests would lead to a resultant low-efficiency operation for both the traction mo-

tor and the engine maps. Therefore, e-assist was used for conditions where the ICE torque was limited, so the traction motor could support demanding accelerations. Regenerative braking was used for any negative acceleration but was limited to the Crate constraints of the battery pack. Each transition threshold was optimized for the different powertrain options in this study. This strategy is commonly used in the literature and has shown similar results compared to more advanced strategies such as an equivalent consumption minimization strategy [31–33]. In addition, the optimization of the different transitions for each of the powertrains provided an effective comparison basis for the architectures.

Different driving conditions comprehending payloads of 0%, 50%, and 100% as well as normative driving cycles such as HWY and WHVC and real driving conditions from different cities were used during this investigation. The real driving profiles were obtained using GT-Real Drive, which fetches real-time traffic information for a given route. Countries representative of three regions were selected: the US, India, and China. For the US, the route Chicago–San Francisco (S-F) was selected whereas for India and China, the routes of Mumbai–Chennai (M-C) and Beijing–Shanghai (B-S) were selected, respectively. The velocity profile for each driving cycle is presented in Figure 5.

(**a**)

(**b**)

(**c**)
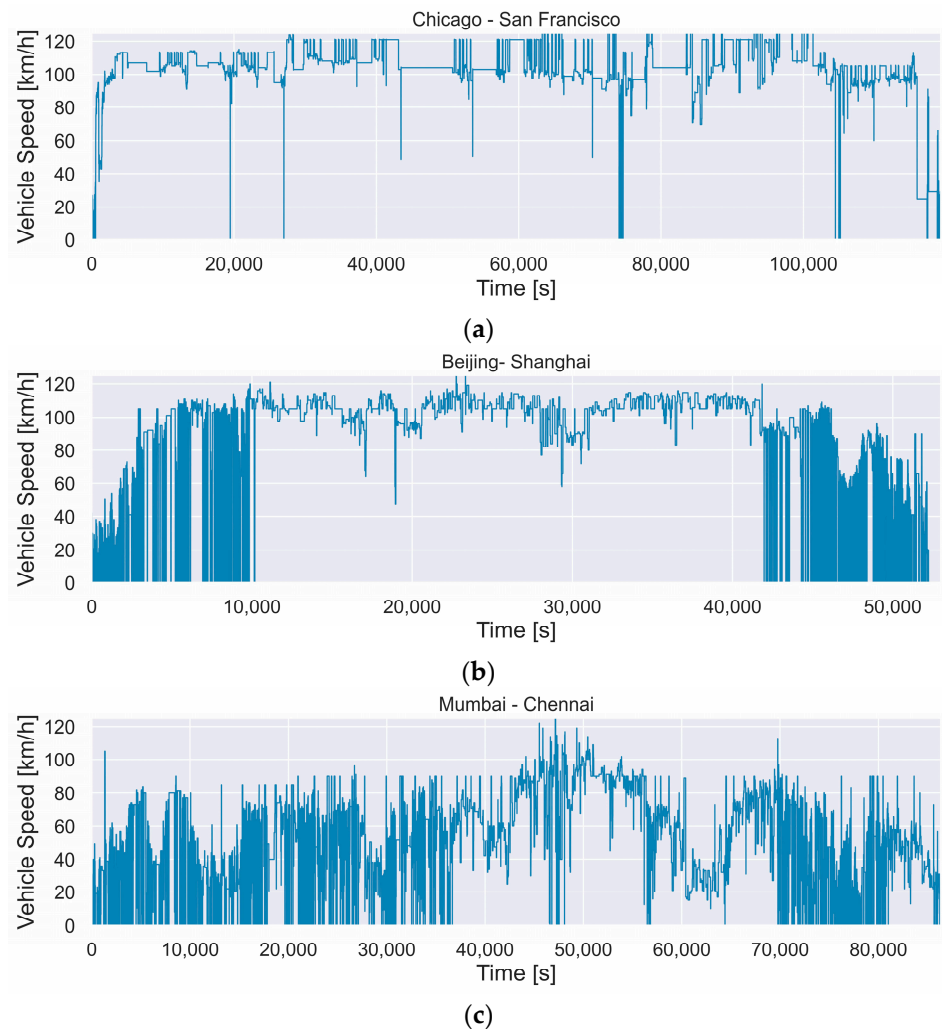
Figure 5. Instantaneous velocity profiles for Chicago–San Francisco (**a**), Beijing–Shanghai (**b**) and Mumbai–Chennai (**c**) driving cycles.

Figure 6 summarizes the steps that were considered in the investigation. It is worth stating that relative differences are presented with the original diesel calibration as reference. Nonetheless, the original maps are not introduced in this work due to confidentiality aspects.
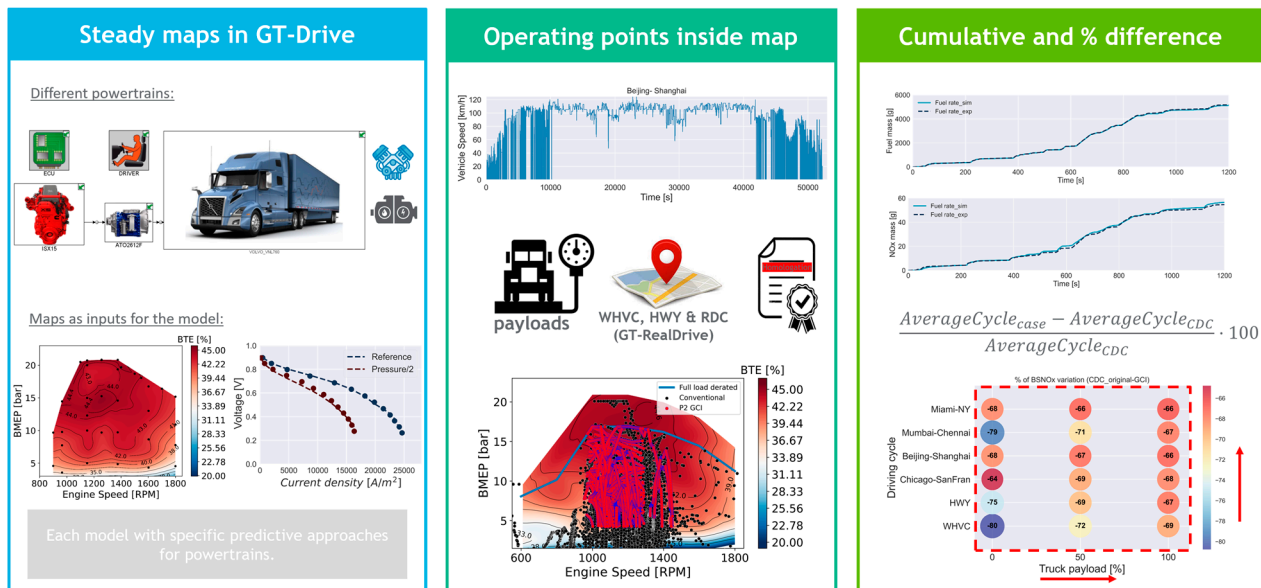
Figure 6. Schematics representing the framework used in the present investigation to assess the different powertrains.

3. Results and Discussion

The results section is divided into three different parts. First, an analysis of the different driving cycles used in this investigation is presented. Later, a study of the effect of the battery size on the performance and emission results of the hybrid powertrain assessed in the WHVC cycle is discussed in detail. Finally, a comparative analysis is performed across different driving conditions, considering emissions, fuel consumption, and the overall CO_2 reduction cost for each powertrain.

3.1. Analysis of the Driving Cycles

To understand the overall differences between each of the driving cycles evaluated, an initial study was performed to quantify the impact of each cycle on brake mean effective pressure, engine speed, and overall power requirements. For this, the conventional powertrain with 50% of the payload was simulated for each cycle.

Figure 7 presents the kernel density estimation plots for engine speed, BMEP, and power during each driving cycle at 50% of the payload. The most probable Gaussian function fitting each parameter's distribution was also used to highlight overall trends. The engine speed results (Figure 7a) illustrate the significant dependence of the engine speed demand with respect to the driving cycles. For example, WHVC presents the lowest requirements in engine speed, caused mainly by the frequent idling during the cycle. In contrast, Chicago–San Francisco presents a more frequent operation around 1300 rpm due to the high portion of the cycle at cruising conditions. Other real driving conditions, such as Beijing–Shanghai, have an engine speed distribution with broader ranges reflecting the mixed urban and highway operation. It is also interesting to note that the engine BMEP is significantly affected by the driving condition at a given payload. The results presented in Figure 7b illustrate that the Mumbai–Chennai driving cycle has one of the lowest load demands, concurring with the vehicle speed profiles previously presented. Such reduced maximum speed is mainly caused by the heavy traffic conditions experienced by the vehicles driving on that route. On the opposite side, Beijing–Shanghai is the most demanding cycle due to the combination of frequent accelerations towards maximum speed in the urban zones and a significant portion of the cycle in cruising conditions. The combination of both engine speed and BMEP provides an overview of the engine power demanded by each cycle, indicating that the 350 kW range of the engine is reached on some occasions, but in general, the distribution peaks are below the 200 kW range.
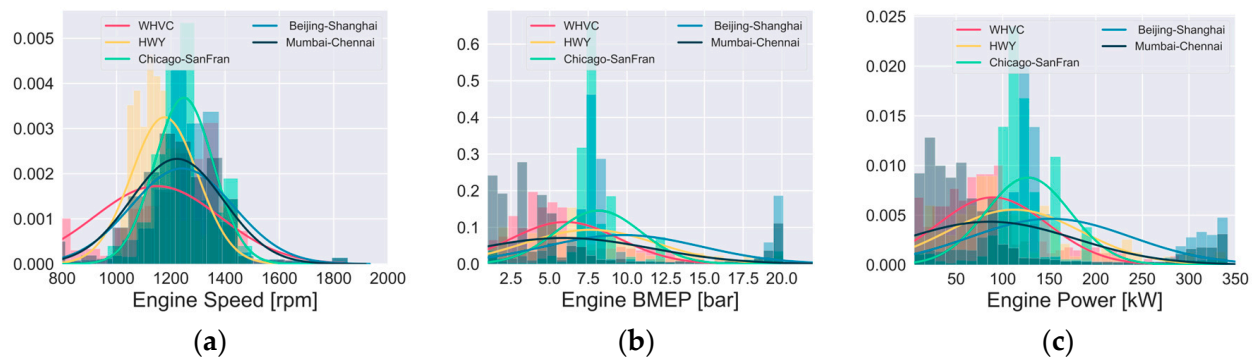
Figure 7. Kernel density estimation and most probable Gaussian functions for engine speed (**a**), brake mean effective pressure (**b**), and engine power (**c**) for the different driving cycles evaluated.

3.2. Battery Size Assessment

The vehicle battery is one of the most critical devices for an efficient hybrid powertrain operation. Proper battery sizing provides extended durability and reduced losses and is an important factor for effective regenerative braking. The battery size dictates the high current limit since the battery Crate specifications must be respected with the risk of overheating and ultimately, thermal runaway if limits are exceeded for extended periods [34,35]. In this sense, parametric sweeps were performed for each of the powertrains to capture the impact of the battery size on the overall system efficiency. Additionally, the secondary objective of this sweep was to determine the best battery size for CO_2 reduction for each application. As discussed in the methodology, for each powertrain, the number of cells in series was swept from 1 to 140. It is worth mentioning that while the P0 and P2 48 V had the same total battery energy, P2 500 V differed since the higher voltage implied a higher total energy. The results are presented as percentage variations compared to the conventional baseline diesel calibration. In this sense, both the optimal battery size and the relative benefits of GCI hybrid powertrains with respect to the original diesel calibration are presented.

Figure 8 depicts the differences in fuel mileage compared to the original diesel calibration for each powertrain assessed. The results show that battery size affects the powertrain mileage differently depending on the payload. For P0 with 0% of the payload, benefits in fuel consumption could be attained to a certain extent as battery size increased. Nonetheless, no significant additional improvement was verified for larger battery sizes. As the payload increased, the sensitivity of the powertrain to the battery size decreased significantly, where case-to-case differences were lower than 3% in absolute values. This is connected to the powertrain's fundamental operation modes that dictate the current drained from the battery. For P0, no e-drive mode was allowed, and the motor size also decreased since most of its requirements were related to start–stop activities and limited regenerative braking. In this sense, the powertrain was never current-limited, and the respective current flow losses were minimized. Due to the same reasons, regenerative braking was not as effective as the other architectures, reducing the overall benefits of fuel consumption reduction. A different scenario was evidenced for the P2 powertrains. It is evident that P2 48 V was current-limited for batteries smaller than 6 kWh for 100% of the payload. This value decreased to below 5 kWh for 0% of the payload due to reduced electric power requirements. It is worth noting that such phenomena can only be captured if a proper battery characterization is included in the simulations by activating dependence maps as a function of the state of charge, temperature, and voltage or fully electrochemistry-based models are applied. The P2 500 V architecture presented a similar behavior compared to the 48 V system. Nonetheless, given the higher voltage of the system, battery capacity increased faster as the number of cells in parallel increased, making it difficult to visualize the phenomena on the x-axis of Figure 8c. The benefits from regenerative braking are also a function of the maximum available energy available considering the optimal braking distribution [32]. Nonetheless, the inclusion of detailed braking strategies for maximum regenerative braking were considered out of the

scope of this work. Therefore, the results account for the maximum regenerative braking, and only limits from the battery management system and traction motors were considered.
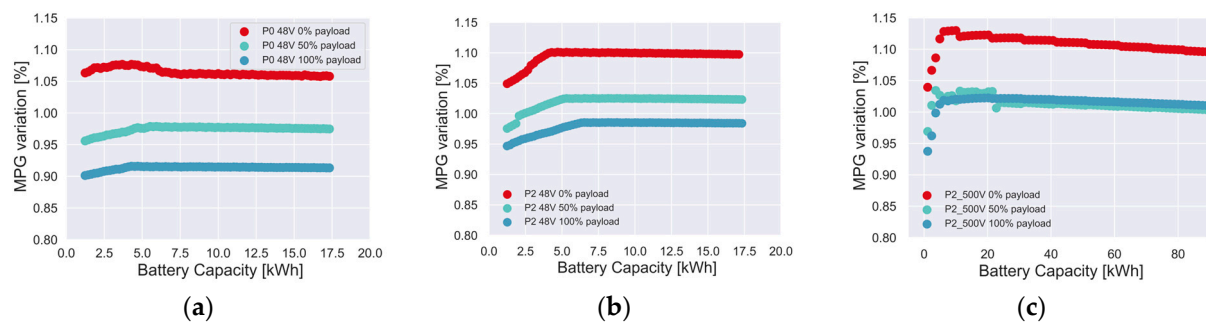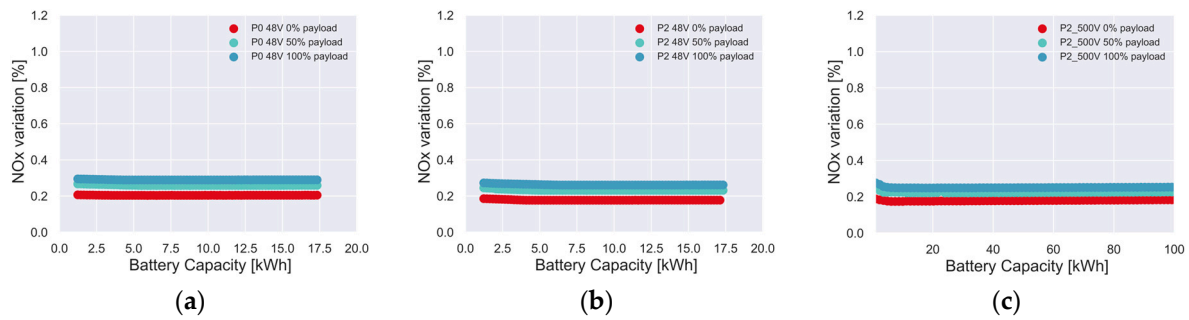

Figure 8. Difference in miles per gallon compared to diesel for P0 48 V (**a**), P2 48 V (**b**), and P2 500 V (**c**) for the WHVC cycle under different payloads.

Overall, P2 500 V benefited from the higher regenerative braking potential and decreased losses in the battery due to reduced current. It is worth mentioning that the benefits of the high powertrain voltage were not fully captured due to the absence of a detailed model for the inverter and power electronics. The potential gains in current reduction can be visualized by comparing the current profiles over the cycle for the same battery size as depicted in Figure 9 below.
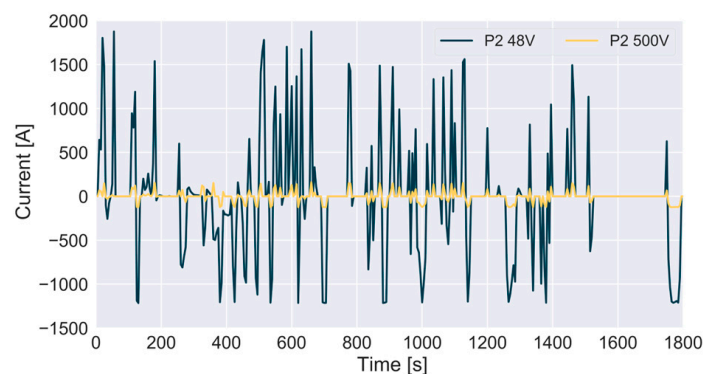

Figure 9. Instantaneous current for P2 in a 48 V and 500 V system during the WHVC cycle with 100% of the payload.

NOx emissions were sensibly reduced for GCI-based powertrains compared to the original calibration. As demonstrated in the methodology section, the NOx calibration target was to be lower than 2 g/kWh at any given condition. Such NOx reduction with small penalizations on fuel consumption was enabled by a dedicated combustion and air management system designed to operate at these conditions, i.e., high EGR values and reduced exhaust enthalpy. In the conventional diesel case, most of the calibrations are designed to provide average RMC SET cycles from 4 to 7 g/kWh, depending on specific conditions, such as current emission legislation targets and the cost of urea used in the SCR system. In this sense, for the whole battery size values investigated, the reductions were beyond 70% as depicted by Figure 10 as a consequence of the low NOx GCI calibration. It can be noted that the payload negatively affected NOx emissions since, in these cases, power requests shifted the truck operating conditions towards higher engine loads. The powertrain effect is also highlighted in the figure. P2 48 V and 500 V showed reduced NOx emissions connected to a lower engine on-time. In addition, the battery size had a similar effect as the one discussed for fuel consumption. A minimum size needs to be respected for these architectures to avoid current-limitation and harness the full potential of the architecture.
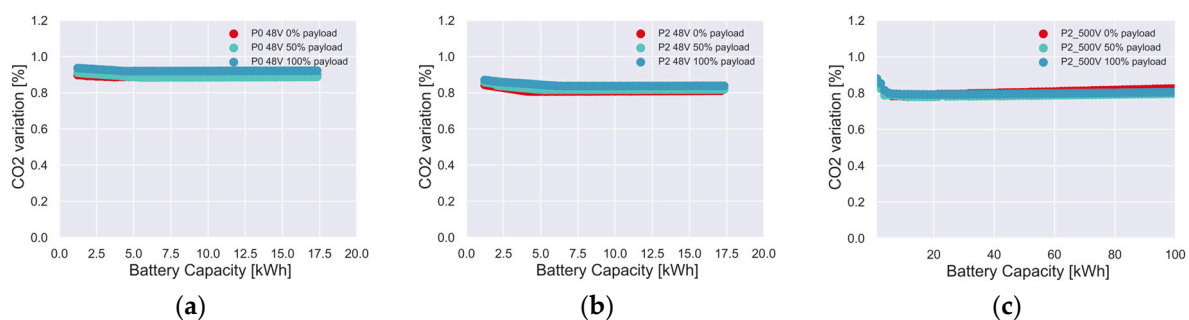
Figure 10. Cumulative nitrogen oxide differences compared to diesel for P0 48 V (**a**), P2 48 V (**b**), and P2 500 V (**c**) for the WHVC cycle under different payloads.

Figure 11 summarizes the results for soot emission reduction over the cycle compared to the original conventional diesel combustion calibration. Both the effect of the calibration and hybrid architecture is shown. While more efficient powertrains were able to achieve higher soot reductions, the dependence on battery size was less significant than the parameters that were previously evaluated. In this case, the differences in the calibration were the main driver mechanism to realize soot reduction. Clearly, GCI calibration excelled, providing reductions of more than 70% for most of the conditions evaluated.
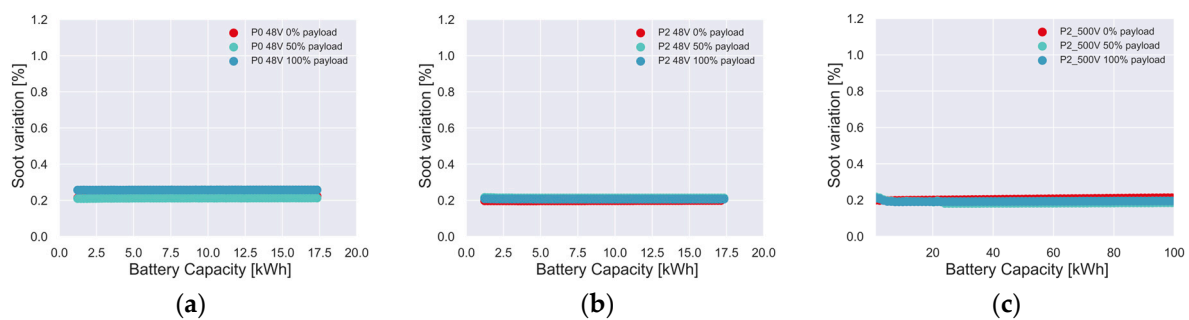
Figure 11. Cumulative soot emission differences compared to diesel for P0 48 V (**a**), P2 48 V (**b**), and P2 500 V (**c**) for the WHVC cycle under different payloads.

Finally, CO_2 results are presented in Figure 12. The absolute reduction in this emission is a consequence of two main mechanisms. First, gasoline has a lower CO_2 formation potential than diesel (3.09 for gasoline compared to 3.16 for diesel) [36]. In addition to this, the energy savings from each powertrain have important contributions. It is clear that P2 had increased gains compared to P0, allowing CO_2 reductions as high as 20% for 0% of the payload. These savings decreased as the payload increased. In addition, it is worth mentioning that no clear benefit could be extracted from extending the battery size towards high-energy packs for the WHVC driving cycle.

Figure 12. Carbon dioxide differences compared to diesel for P0 48 V (**a**), P2 48 V (**b**), and P2 500 V (**c**) for the WHVC cycle under different payloads.

Considering the results of fuel consumption, emissions, and CO_2, a final battery size selection of 6 kWh, 7.2 kWh, and 20 kWh was used for the global comparison of each powertrain and to obtain the overall powertrain performance under different driving conditions that is presented in the next section.

3.3. Performance and Emission Results for Different Driving Conditions

This subsection compares GCI hybrid powertrains with a conventional truck under different driving conditions. Later, each powertrain cost is also considered and used to understand the cost for the CO_2 reduction of each concept.

3.3.1. Performance and Emission Results

This section summarizes the impacts of driving conditions, i.e., driving cycles and payloads on fuel consumption, NOx, and CO_2 emissions. Differently from the previous section, the results are compared with the conventional truck running with the baseline GCI calibration instead of diesel. In this sense, the effect of the hybrid powertrains can be isolated. Figure 13 presents the impact of the different hybridization levels on the fuel mileage of the truck for the different conditions that were assessed. Evidently, there is a significant spread in the values for each powertrain. The WHVC driving cycle suggests increased benefits for P2 hybrids over P0. While P0 can support limited regenerative braking, the smaller motor size cannot harness the extra energy from high payload cases. P2 48 V and 500 V excel at these conditions, with fuel consumption savings of more than 10% on an absolute basis compared to P0 for the WHVC cycle with a 100% payload.
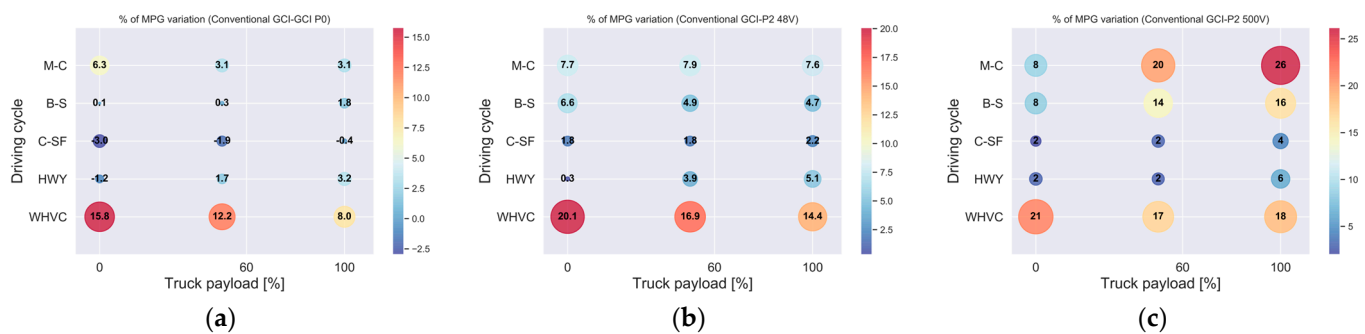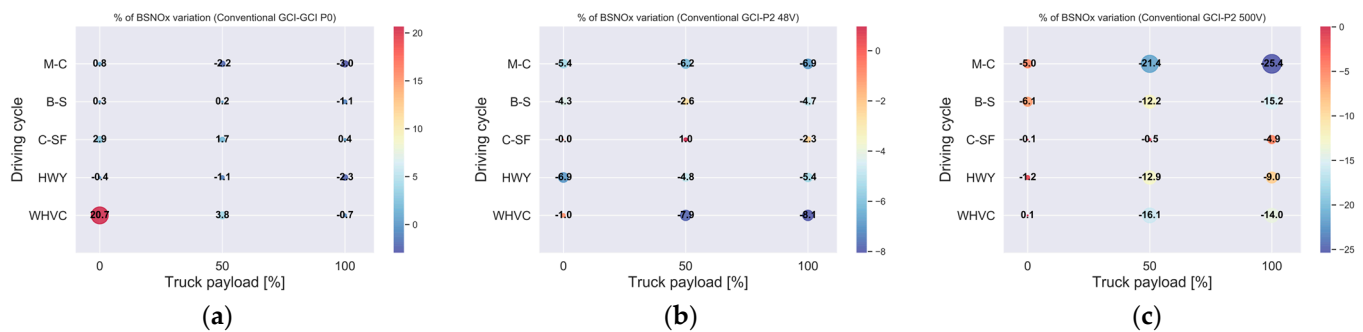

Figure 13. Summary plots representing the variation in miles per gallon compared to the gasoline compression ignition combustion calibration for P0 48 V (**a**), P2 48 V (**b**), and P2 500 V (**c**) for the different driving cycles and payloads evaluated.

It is interesting to note that demanding driving cycles with limited regenerative braking opportunities significantly constrain hybridization's benefits. Both highway (HWY) and Chicago–San Francisco driving cycles present maximum benefits of 6% for the P2 500 V cases. It can be argued that the benefits of a high hybridization level may not pay off compared to P2 and P0 48 V since both can have similar benefits. Beijing–Shanghai, a mixed cycle with two urban phases, enables higher fuel consumption savings. Given the limited battery and motor capacity, this can only partially be extracted by the 48 V architectures. Conversely, P2 500 V can achieve more than 15% fuel consumption improvements. A similar behavior is also evidenced in the Mumbai–Chennai case in India. The highly transient cycle with limited maximum speeds favors the use of strong hybridization, allowing the recovery of a significant portion of the braking energy without exceeding the motor and Crate capacities of the powertrain.

The impact of powertrain hybridization on NOx emissions was also assessed and compared under the different driving conditions used in this investigation. In general, as it is shown in Figure 14, P0 did not reduce NOx emissions compared to the conventional GCI powertrain. This can be attributed to the absence of an e-drive mode, indicating that the internal combustion engine provides all of the traction energy. It is worth remembering

that the variations observed in NOx emissions presented in Figure 14 are in addition to the initial benefits from using GCI over conventional diesel combustion that can be as high as 80%, as demonstrated in the battery size investigation in Section 3.2.

Figure 14. Summary plots representing the variation in NOx emissions compared to the gasoline compression ignition combustion calibration for P0 48 V (**a**), P2 48 V (**b**), and P2 500 V (**c**) for the different driving cycles and payloads evaluated.

The use of P2-based powertrains unlocks additional savings in NOx emissions, mainly from the ability to electrically drive the powertrain. While P2 48 V can provide benefits as high as 7%, the 500 V platform generates benefits of over 25% for the India driving cycle under elevated payloads. It is worth mentioning that get-hot and stay-hot conditions are challenged using strong hybridization given the frequent engine-off times. In this case, alternatives based on the use of electrical heated catalyst or other light-off enhancing and thermal management techniques will be required and should be further investigated to minimize the impact on tailpipe pollutants.

Finally, the impact of powertrain hybridization on tank-to-wheel CO_2 emissions is also shown for the different truck payloads and driving cycles in Figure 15. As expected, CO_2 tank-to-wheel emissions closely follow the values found for fuel consumption. This correlation always exists from an engine-out perspective, except in cases where unburned hydrocarbons and carbon monoxide emissions are excessively high. This could lead to a misreport of CO_2 emissions since the final goal is to convert them into oxidation catalysts where the final product would be CO_2. Again, it is worth remarking the superior ability of P2 to reduce the vehicle's carbon footprint for conditions where regenerative braking opportunities are abundant. Nonetheless, limited benefits in CO_2 emissions are found for highway-based driving cycles. In these cases, low hybridization levels can provide similar CO_2 benefits as P2 500 V from fuel consumption and CO_2 and NOx perspectives. Additionally, 48 V would also enable the use of auxiliary electric devices to support powertrain efficiencies, such as an e-booster, e-EGR pump, and heaters for the after treatment, which are key to achieving future legislation targets for criteria pollutants.
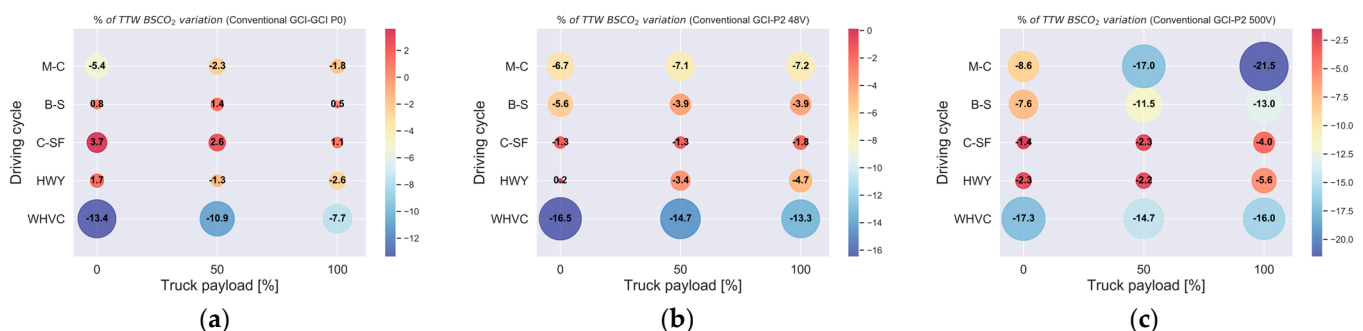
Figure 15. Summary plots representing the variation in CO_2 emissions compared to the gasoline compression ignition combustion calibration for P0 48 V (**a**), P2 48 V (**b**), and P2 500 V (**c**) for the different driving cycles and payloads evaluated.

3.3.2. CO_2 Reduction Cost

As previously discussed, each powertrain can enable different CO_2 savings that depend on the battery and motor size and the limits on regenerative braking. Higher CO_2 reductions were experienced on powertrains with higher hybridization levels in drive cycles involving frequent vehicle transients. Nonetheless, additional costs associated with the manufacturing process could imply a higher purchase cost for the consumer. Therefore, an additional cost analysis was performed to understand the overall cost increase of each powertrain and provide a relationship between the CO_2 savings and the associated market purchase price. For that, the mean sales retail price (MSRP) of the truck was calculated considering the values proposed by [37], which are presented in Table 5 below and multiplied by a flat rate of 1.2.

Table 5. Associated costs for different powertrain components.

Parts	Cost
Glider [USD]	120,000
Engine [USD/kWh]	48
Battery [USD/kWh]	190
Power electronics [USD/kW]	50

In sequence, Table 6 illustrates the final MSRP for each of the powertrain architectures investigated, considering the values from Table 5. As can be seen, mild hybridization represents the smallest increase in vehicle price compared to baseline vehicle, whereas high hybridization levels represent a purchase cost of around 30% higher.

**Table 6.** MSRP for each of the powertrains considered in the investigation.

Powertrain	Retail Price [USD]	Difference [%]
Conventional	163,740	-
P0 48 V	166,836	1.89
P2 48 V	171,492	4.73
P2 500 V	211,260	29.02

Considering that the same powertrain is used across different markets, the overall cost per CO_2 reduction can be obtained, understanding that power requirements in the Indian market enable the use of smaller engines and can be an alternative for cost saving. Nonetheless, this vehicle sizing exercise was considered out of the scope of this investigation.

Figure 16 summarizes the economic impact of each powertrain for the obtained CO_2 reduction across the different markets assessed. The truck payload was used to separate each graph, allowing to capture the effect of the driving condition and payload on the overall cost versus CO_2 trade-off. It is worth mentioning for the sake of clarity that the comparison was made by considering the original diesel engine calibration as baseline. Therefore, the potential of hybrid GCI powertrains could be captured as a possible alternative to conventional diesel trucks.

As shown, there are small variations in the overall CO_2 savings with respect to the increased cost (consequently, powertrain) for 0% of the truck payload. As the load increases, differences in each market are evidenced. While US cycles (HWY and Chicago–San Francisco) have low benefits from any of the hybrid powertrains, India, China, and WHVC cycles (Europe) benefit from a strong hybridization from a CO_2 savings perspective. In cases where regenerative braking is limited (P0 layout on Chicago–San Francisco and Beijing–Shanghai), the conventional diesel powertrain shows the benefits of the hybridized platform from a CO_2 perspective and cost trade-off. An additional cost analysis should consider fines, taxes and tolls benefits, fuel consumption throughout the vehicle life, and other financial parameters to capture the overall picture of each powertrain in a total cost of ownership analysis. Nonetheless, the results provided in Figure 16 shed light on the

importance of considering the particularities of each market and their overall benefits on the partial electrification of the powertrain. Other technologies such as fuel cells or low-carbon fuels for internal combustion engines can be a more effective way to reduce the carbon footprint for the class 8 sector in these specific markets.
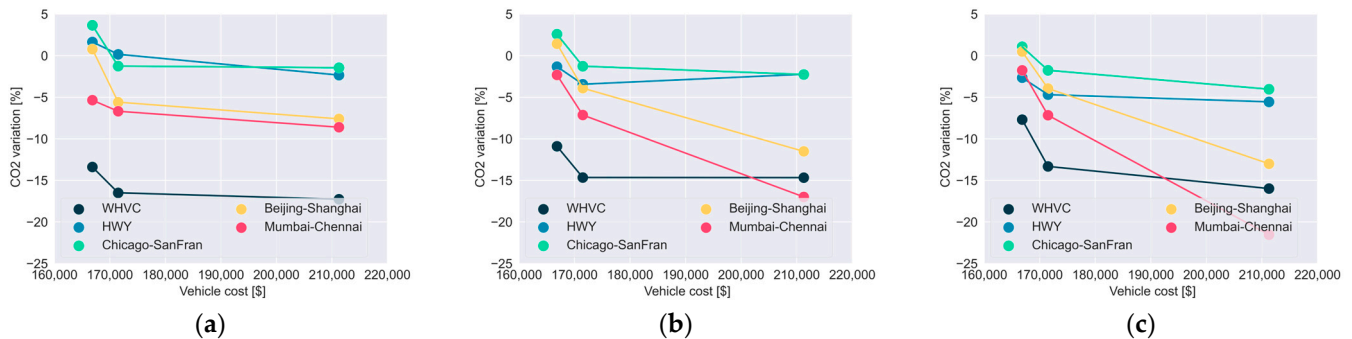
Figure 16. CO_2 benefits versus vehicle cost at different driving cycles for 0% (**a**), 50% (**b**), and 100% (**c**) of the payload.

4. Conclusions

This work performed a detailed investigation considering the combined use of gasoline compression ignition combustion with hybrid powertrains under different driving conditions from the US, India, China, and Europe. Important conclusions and takeaways were identified:

- Gasoline compression ignition can effectively reduce soot and NOx emissions across the board while maintaining similar efficiency levels to the conventional diesel combustion calibration. The combined use of hybridization and GCI can enable reductions higher than 80% for both soot and NOx for the WHVC cycle at 50% of the engine load.
- Battery sizing has a significant effect on the overall vehicle fuel consumption. The electrochemistry limitations of the battery cell must be respected to avoid overheating and further consequences such as the occurrence of thermal runaway.
- The overall powertrain performance is strongly connected to the drive cycle and payload. It was observed that limited benefits were obtained on highway-based conditions, whereas highly transient cycles benefited from strong hybridization. This indicates the need for a correct and detailed powertrain design for each market.
- Hybridization did not demonstrate strong effects on nitrogen oxide emissions, where most of the limited benefits were attributed to a reduced use of the internal combustion engine for which electric drive was available.
- The cost–CO_2 reduction trade-offs highlighted that specific markets may not be suitable for strong hybridization, where 48 V platforms may already provide the required flexibility for regenerative braking, and to support electric systems such as e-turbochargers, e-EGR pumps, and electrically heated catalysts.

Considering the results obtained in this investigation, it is evident that hybridization benefits the overall vehicle operation from an efficiency and emission perspective. Nonetheless, each hybrid powertrain will respond differently to the conditions of a given market, i.e., driving patterns and allowed payloads. In this sense, it can be concluded that the proposed framework is an effective tool to understand overall powertrain performance in a given market and enable informed decisions on component sizing and expected fuel consumption and emission benefits.

Author Contributions: Conceptualization, Y.Z. and P.K.; methodology, R.L.S.; validation, B.M.; formal analysis, R.L.S., Y.Z., P.K. and A.S.; investigation, R.L.S. and B.M.; data curation, B.M.; writing—original draft preparation, R.L.S.; writing—review and editing, Y.Z., P.K. and A.S.; supervision, Y.Z. All authors have read and agreed to the published version of the manuscript.

Data Availability Statement: The data presented in this study are available on request from the corresponding author.

Conflicts of Interest: The authors declare no conflict of interest.

Abbreviations

BAS	Belted alternator starter
BEV	Battery electric vehicle
BSFC	Brake-specific fuel consumption
BSNOx	Brake-specific NOx emissions
BSSoot	Brake-specific soot emissions
CDC	Conventional diesel combustion
CO	Carbon monoxide
CO2	Carbon dioxide
DMDF	Dual-mode dual-fuel combustion mode
EGR	Exhaust gas recirculation
EUVI	EURO VI legislation
FSN	Filter smoke number
FTP	Federal test procedure
GCI	Gasoline compression ignition
HC	Unburned hydrocarbons
HP EGR	High-pressure EGR circuit
HWY	Highway
ICE	Internal combustion engine
LP EGR	Low-pressure EGR circuit
MHEV	Mild hybrid electric vehicle
MSRP	Mean sales retail price
NOx	Nitrogen oxides
OFTA	One factor at a time
PPCI	Partially premixed compression ignition
RBC	Rule-based controller
RCCI	Reactivity-controlled compression ignition
SET	Supplementary engine test
SOC	State of charge
TRL	Technology readiness levels
WHVC	World-harmonized vehicle cycle

References

1. Muncrief, R.; Sharpe, B. *Overview of the Heavy-Duty Vehicle Market and CO2 Emissions in the European Union*; International Council on Clean Transportation: Washington, DC, USA, 2015; pp. 1–14.
2. Lattanzio, R.K. *Heavy-Duty Vehicles, Air Pollution, and Climate Change 2023*; Congressional Research Service: Washington, DC, USA, 2023; pp. 14–16.
3. DieselNet United States: Heavy-Duty Vehicles: GHG Emissions & Fuel Economy. Available online: https://dieselnet.com/standards/us/fe_hd.php (accessed on 11 December 2023).
4. The European Commission Regulations. Commission Regulations (EU) 2019/318 of February 2019 Amending Regulation (EU) 2017/2400 and Directive 2007/46/EC of the European Parliament and of the Council as Regards the Determination of the CO2 Emission and Fuel Consumption of Heavy-Duty. *Off. J. Eur. Union* **2019**, *2001*, 20–30.
5. Molina, S.; García, A.; Monsalve-Serrano, J.; Estepa, D. Miller Cycle for Improved Efficiency, Load Range and Emissions in a Heavy-Duty Engine Running under Reactivity Controlled Compression Ignition Combustion. *Appl. Therm. Eng.* **2018**, *136*, 161–168. [CrossRef]
6. Splitter, D.; Hanson, R.; Kokjohn, S.; Reitz, R. Reactivity Controlled Compression Ignition (RCCI) Heavy-Duty Engine Operation at Mid-and High-Loads with Conventional and Alternative Fuels. In *Proceedings of the SAE 2011 World Congress and Exhibition*; SAE International: Warrendale, PA, USA, 2011. [CrossRef]
7. Pedrozo, V.B.; May, I.; Zhao, H. Exploring the Mid-Load Potential of Ethanol-Diesel Dual-Fuel Combustion with and without EGR. *Appl. Energy* **2017**, *193*, 263–275. [CrossRef]
8. García, A.; Monsalve-Serrano, J.; Lago Sari, R.; Gaillard, P. Assessment of a Complete Truck Operating under Dual-Mode Dual-Fuel Combustion in Real Life Applications: Performance and Emissions Analysis. *Appl. Energy* **2020**, *279*, 115729. [CrossRef]

9.   García, A.; Monsalve-Serrano, J.; Lago Sari, R.; Fogué-Robles, Á. Use of EGR E-Pump for Dual-Mode Dual-Fuel Engines in Mild Hybrid Architectures. *Energy Convers. Manag.* **2021**, *247*, 114701. [CrossRef]

10.   García, A.; Monsalve-Serrano, J.; Villalta, D.; Sari, R. Octane Number Influence on Combustion and Performance Parameters in a Dual-Mode Dual-Fuel Engine. *Fuel* **2019**, *258*, 116140. [CrossRef]

11.   Benajes, J.; García, A.; Monsalve-Serrano, J.; Sari, R. Clean and Efficient Dual-Fuel Combustion Using OMEx as High Reactivity Fuel: Comparison to Diesel-Gasoline Calibration. *Energy Convers. Manag.* **2020**, *216*, 112953. [CrossRef]

12.   Poussin, O.; Gaillard, P.; Garcia, A.; Monsalve-Serrano, J.; Martinez-Boggio, S.D. Dual-Fuel RCCI Diesel-Gasoline Hybrid Truck Concept to Achieve the Future Emissions Targets. In Proceedings of the 10th Aachen Colloquium China Sustainable Mobility, online, 5–7 October 2020.

13.   García, A.; Monsalve-Serrano, J.; Lago Sari, R.; Martinez-Boggio, S. Energy Assessment of an Electrically Heated Catalyst in a Hybrid RCCI Truck. *Energy* **2022**, *238*, 121681. [CrossRef]

14.   Zhang, Y.; Kumar, P.; Pei, Y.; Traver, M.; Popuri, S. *An Experimental and Computational Investigation of Gasoline Compression Ignition Using Conventional and Higher Reactivity Gasolines in a Multi-Cylinder Heavy-Duty Diesel Engine*; SAE Technical Paper; SAE International: Warrendale, PA, USA, 2018. [CrossRef]

15.   Torelli, R.; National, A.; Pei, Y.; Zhang, Y.; Traver, M.; Sellnau, M.; Som, S.; National, A. *Effect of Fuel Temperature on the Performance of a Heavy-Duty Diesel Injector Operating with Gasoline*; SAE International: Warrendale, PA, USA, 2021; pp. 1–11. [CrossRef]

16.   Kavuri, C.; Paz, J.; Kokjohn, S.L. A Comparison of Reactivity Controlled Compression Ignition (RCCI) and Gasoline Compression Ignition (GCI) Strategies at High Load, Low Speed Conditions. *Energy Convers. Manag.* **2016**, *127*, 324–341. [CrossRef]

17.   Putrasari, Y.; Lim, O. A Review of Gasoline Compression Ignition: A Promising Technology Potentially Fueled with Mixtures of Gasoline and Biodiesel to Meet Future Engine Efficiency and Emission Targets. *Energies* **2019**, *12*, 238. [CrossRef]

18.   Kumar, P.; Zhang, Y. Variable Valve Strategy Evaluation for Low-Load Operation in a Heavy-Duty Gasoline Compression Ignition Engine. *Energies* **2022**, *15*, 2017. [CrossRef]

19.   Zhang, Y.; Kumar, P.; Pei, Y.; Traver, M.; Popuri, S. An Experimental and Computational Investigation of Tai-lor-Developed Combustion and Air-Handling System Concepts in a Heavy-Duty Gasoline Compression Ignition Engine. *Energies* **2022**, *15*, 1087. [CrossRef]

20.   Bouter, A.; Hache, E.; Ternel, C.; Beauchet, S. Comparative Environmental Life Cycle Assessment of Several Powertrain Types for Cars and Buses in France for Two Driving Cycles: "Worldwide Harmonized Light Vehicle Test Procedure" Cycle and Urban Cycle. *Int. J. Life Cycle Assess.* **2020**, *25*, 1545–1565. [CrossRef]

21.   Lawler, B.; Ortiz-Soto, E.; Gupta, R.; Peng, H.; Filipi, Z. Hybrid Electric Vehicle Powertrain and Control Strategy Optimization to Maximize the Synergy with a Gasoline HCCI Engine. *SAE Int. J. Engines* **2011**, *4*, 1115–1126. [CrossRef]

22.   Hanson, R.; Curran, S.; Spannbauer, S.; Storey, J.; Huff, S.; Gross, C.; Reitz, R. Fuel Economy and Emissions Testing of an RCCI Series Hybrid Vehicle. *Int. J. Powertrains* **2017**, *6*, 259–281. [CrossRef]

23.   Luján, J.M.; García, A.; Monsalve-Serrano, J.; Martínez-Boggio, S. Effectiveness of Hybrid Powertrains to Reduce the Fuel Consumption and NOx Emissions of a Euro 6d-Temp Diesel Engine under Real-Life Driving Conditions. *Energy Convers. Manag.* **2019**, *199*, 111987. [CrossRef]

24.   García, A.; Monsalve-Serrano, J.; Martínez-Boggio, S.; Wittek, K. Potential of Hybrid Powertrains in a Variable Compression Ratio Downsized Turbocharged VVA Spark Ignition Engine. *Energy* **2020**, *195*, 117039. [CrossRef]

25.   Nieto Prada, D.; Vijayagopal, R.; Costanzo, V. *Opportunities for Medium and Heavy Duty Vehicle Fuel Economy Improvements through Hybridization*; SAE Technical Papers; SAE International: Warrendale, PA, USA, 2021; pp. 1–14. [CrossRef]

26.   Zhao, H.; Burke, A.; Miller, M. Analysis of Class 8 Truck Technologies for Their Fuel Savings and Economics. *Transp. Res. D Transp. Environ.* **2013**, *23*, 55–63. [CrossRef]

27.   García, A.; Monsalve-Serrano, J.; Martinez-Boggio, S.; Gaillard, P.; Poussin, O.; Amer, A.A. Dual Fuel Combustion and Hybrid Electric Powertrains as Potential Solution to Achieve 2025 Emissions Targets in Medium Duty Trucks Sector. *Energy Convers Manag.* **2020**, *224*, 113320. [CrossRef]

28.   Zhao, H.; Burke, A.; Zhu, L. Analysis of Class 8 Hybrid-Electric Truck Technologies Using Diesel, LNG, Electricity, and Hydrogen, as the Fuel for Various Applications. In Proceedings of the 2013 World Electric Vehicle Symposium and Exhibition, EVS 2013, Barcelona, Spain, 17–20 November 2013; pp. 1–16. [CrossRef]

29.   Balazadeh Meresht, N.; Moghadasi, S.; Munshi, S.; Shahbakhti, M.; McTaggart-Cowan, G. Advances in Vehicle and Powertrain Efficiency of Long-Haul Commercial Vehicles: A Review. *Energies* **2023**, *16*, 6809. [CrossRef]

30.   Gamma Technologies. *Vehicle_Driveline_and_HEV Application Manual*; Gamma Technologies, Inc.: Westmont, IL, USA, 2016.

31.   Sorrentino, M.; Rizzo, G.; Arsie, I. Analysis of a Rule-Based Control Strategy for on-Board Energy Management of Series Hybrid Vehicles. *Control Eng. Pract.* **2011**, *19*, 1433–1441. [CrossRef]

32.   Caratozzolo, P.; Serra, M.; Riera, J. Energy Management Strategies for Hybrid Electric Vehicles. In Proceedings of the IEMDC 2003—IEEE International Electric Machines and Drives Conference, Madison, WI, USA, 1–4 June 2003; Volume 1, pp. 241–248. [CrossRef]

33.   Nguyen, B.H.; Trovao, J.P.; German, R.; Bouscayrol, A.; Goulet, Y. Optimal Energy Management of a Parallel Hybrid Truck for Fuel Consumption Comparative Study. In Proceedings of the IEEE Vehicular Technology Conference 2018, Porto, Portugal, 3–6 June 2018; pp. 1–5. [CrossRef]

34. Feng, X.; He, X.; Ouyang, M.; Wang, L.; Lu, L.; Ren, D.; Santhanagopalan, S. A Coupled Electrochemical-Thermal Failure Model for Predicting the Thermal Runaway Behavior of Lithium-Ion Batteries. *J. Electrochem. Soc.* **2018**, *165*, A3748–A3765. [CrossRef]
35. Garcia, A.; Monsalve-serrano, J.; Sari, R. Identifying Key Aspects of Thermal Runaway Modelling for Lithium-Ion Battery Cells. *SAE Int. J. Adv. Curr. Pract. Mobil.* **2022**, *4*, 1964–1976. [CrossRef]
36. Benajes, J.; García, A.; Monsalve-Serrano, J.; Martínez-Boggio, S. Potential of Using OMEx as Substitute of Diesel in the Dual-Fuel Combustion Mode to Reduce the Global CO_2 Emissions. *Transp. Eng.* **2020**, *1*, 100001. [CrossRef]
37. Hunter, C.; Penev, M. *Market Segmentation Analysis of Medium and Heavy Duty Trucks with a Fuel Cell Emphasis Fuel Cell M/HD Vehicle Market Segmentation*; National Renewable Energy Lab. (NREL): Golden, CO, USA, 2019; pp. 1–6.